Effects of Ionizable Residues on the Absorption Spectrum and Initial Electron-Transfer Kinetics in the Photosynthetic Reaction Center of *Rhodobacter sphaeroides*†

E. T. Johnson,‡,§ V. Nagarajan,‡ V. Zazubovich,|| K. Riley,|| G. J. Small,|| and W. W. Parson*,‡

Department of Biochemistry, Box 357350, University of Washington, Seattle, Washington 98195-7350, and Ames Laboratory-USDOE and Department of Chemistry, Iowa State University, Ames, Iowa 50011

Received August 1, 2003; Revised Manuscript Received September 24, 2003

ABSTRACT: Effects of ionizable amino acids on spectroscopic properties and electron-transfer kinetics in the photosynthetic reaction center (RC) of *Rhodobacter sphaeroides* are investigated by site-directed mutations designed to alter the electrostatic environment of the bacteriochlorophyll dimer that serves as the photochemical electron donor (P). Arginine residues at homologous positions in the L and M subunits (L135 and M164) are changed independently: Arg L135 is replaced by Lys, Leu, Glu, and Gln and Arg M164 by Leu and Glu. Asp L155 also is mutated to Asn, Tyr L164 to Phe, and Cys L247 to Lys and Asp. The mutations at L155, L164, and M164 have little effect on the absorption spectrum, whereas those at L135 and L247 shift the long-wavelength absorption band of P to higher energies. Fits to the ground-state absorption and hole-burned spectra indicate that the blue shift and increased width of the absorption band in the L135 mutants are due partly to changes in the distribution of energies for the zero-phonon absorption line and partly to stronger electron−phonon coupling. The initial electron-transfer kinetics are not changed significantly in most of the mutants, but the time constant increases from 3.0 ± 0.2 in wild-type RCs to 4.7 ± 0.2 in C(L247)D and 7.0 ± 0.3 ps in C(L247)K. The effects of the mutations on the solvation free energies of the product of the initial electron-transfer reaction ($P^+B_L^-$) and the charge-transfer states that contribute to the absorption spectrum ($P_L^+P_M^-$ and $P_L^-P_M^+$) were calculated by using a distance-dependent electrostatic screening factor. The results are qualitatively in accord with the view that electrostatic interactions of the bacteriochlorophylls with ionized residues of the protein are strongly screened and make only minor contributions to the energetics and dynamics of charge separation. However, the slowing of electron transfer in the Cys L247 mutants and the blue shift of the spectrum in some of the Arg L135 and Cys L247 mutants cannot be explained consistently by electrostatic interactions of the mutated residues with P and B_L; we ascribe these effects tentatively to structural changes caused by the mutations.

The bacteriochlorophyll (Bchl)[1] and bacteriopheophytin (Bphe) molecules that participate in the initial electron-transfer steps in photosynthetic reaction centers (RCs) of *Rhodobacter sphaeroides* are bound to two homologous subunits (L and M), which form a complex with noncrystallographic 2-fold symmetry (*1*). Upon photoexcitation, a special pair of strongly interacting Bchls (P) transfers an electron through an accessory Bchl (B_L) to a Bphe (H_L). Despite the symmetry of the structure, electron transfer occurs predominantly to the pigments on the L side of the RC, forming the $P^+B_L^-$ and $P^+H_L^-$ ion pairs in preference to the corresponding products on the M side ($P^+B_M^-$ and $P^+H_M^-$). A difference between the energies of $P^+B_L^-$ and $P^+B_M^-$ probably accounts for much of the asymmetry of the electron-transfer reaction (*2*−*4*), although the electronic coupling factors also appear to differ on the two sides (*5*−*7*).

A variety of mutations that change the energies of the ion-pair states have been found to alter the electron-transfer kinetics in bacterial RCs. Mutations that introduce hydrogen bonds to the carbonyl groups of the Bchls of P (P_L or P_M) generally destabilize P^+ and slow the initial electron-transfer reaction (*8*, *9*). Conversely, replacing a nearby Asn residue by Asp can stabilize P^+ and speed the reaction (*10*, *11*). Replacing Tyr M210 by a Phe removes a hydroxyl group that stabilizes $P^+B_L^-$, again decreasing the rate of electron

† Work at the University of Washington was supported by National Science Foundation Grants MCB-9904618 and MCB-0236149 and a Molecular Biophysics Training Grant (GM08268) from the National Institutes of Health. Research at the Ames Laboratory was supported by the Division of Chemical Sciences, Office of Basic Energy Sciences, U. S. Department of Energy. Ames Laboratory is operated for the USDOE by Iowa State University under Contract W-7405-Eng-82.

* Corresponding author. E-mail: parsonb@u.washington.edu. Phone: (206) 543-1743. Fax: (206) 685-1792.

‡ University of Washington.

§ Present address: Pacific Northwest National Lab, P.O. Box 999/MS K8-98, Richland, WA 99352.

|| Iowa State University.

[1] Abbreviations: Bchl, bacteriochlorophyll; Bphe, bacteriopheophytin; E_m, midpoint reduction potential; fwhm, full width at half-maximum amplitude; LDAO, lauryldimethylamine-*N*-oxide; RC, reaction center; P, the special pair of Bchls that acts as the photochemical electron donor; B_L and H_L, Bchl and Bphe molecules that serve as electron acceptors; SDF, site-distribution function; WT, wild-type; ZPH, zero-phonon hole; ZPL, zero-phonon line.

10.1021/bi035366d CCC: $25.00
Published on Web 10/30/2003

transfer (*12*−*16*). Heller et al. (*17*) have shown that introducing an Asp residue near B_L slows the kinetics, probably by destabilizing $P^+B_L^-$, and Katilius et al. (*18*) have described a mutation that speeds up electron transfer to B_M, probably by stabilizing $P^+B_M^-$. However, all these studies focus on residues that are in close proximity to the Bchls. In principle, mutations of these residues could perturb the positions or molecular orbitals of the Bchls, making it difficult to isolate effects on the electrostatic energies. The effects of long-range electrostatic interactions with more distant residues remain largely unexplored. Several theoretical studies (*19*, *20*) have suggested that static electric fields from ionized amino acid side chains play important roles in this regard. However, other work (*10*, *21*−*23*) indicates that electrostatic interactions of the pigments with the ionized groups are strongly screened by the solvent, electrolytes, and induced dipoles in the protein.

The electronic absorption spectrum of RCs has been studied extensively for insight into the electronic properties of the complex. At room temperature, wild-type (WT) RCs have a strong absorption band near 870 nm that can be assigned almost exclusively to P, a band near 800 nm due to B_L and B_M with some contributions from P, and a band at 760 nm due to H_L and H_M. We will refer to the low-energy absorption band as the P870 band for simplicity, although it shifts to longer wavelengths at cryogenic temperatures. The P870 band consists mainly of an antisymmetric combination of the $S_0 \rightarrow S_1$ (Q_y) transitions of P_L and P_M. However, electron-exchange coupling of P_L and P_M leads to charge-transfer (CT) transitions that borrow some of the intensity of the P870 band and shift it strongly to the red (*24*, *25*). This coupling endows the P870 band with appreciable CT character that is manifested by a strong Stark effect. Stark spectroscopy experiments indicate that the change in the permanent dipole moment associated with the optical transition ($|\Delta\mu|$) is on the order of 5 D, which is about 5 times larger than the $|\Delta\mu|$ observed for a Q_y transition localized on a single Bchl-*a* molecule (*26*−*29*). The spectroscopic effects of the hydrogen-bond mutations mentioned previously have been explored and have been rationalized as reflecting changes in the energy of the $P_L^+P_M^-$ CT state (*8*, *30*−*34*). Effects of mutations that change the orientation of the acetyl group of P_L have been described (*35*). Changes in detergents or ionic strength also can affect the P870 band (*36*−*39*). Again, however, there is little quantitative information on how long-range electrostatic interactions affect the spectrum.

In previous studies, we found that mutations of ionizable residues located 10−15 Å from P alter the distribution of the unpaired electron spin of P^+ between P_L and P_M (*23*) but cause only small shifts in the E_m of P/P^+ (*22*) and the IR absorption spectrum of P^+ (*23*). Here, we explore how these mutations affect the ground-state absorption spectrum, the hole-burned spectrum at 5 K, and the initial electron-transfer kinetics.

MATERIALS AND METHODS

Construction of Mutants and Purification of RCs. Oligonucleotide-mediated site-directed mutagenesis was accomplished as described (*22*, *23*). DNA from each strain was purified and sequenced to ensure that the mutations had been introduced correctly.

R. sphaeroides was grown semi-aerobically in rich media for 3−5 days in the dark (*40*). Reaction centers were isolated by standard procedures (*41*, *42*) with minor modifications as described (*22*, *23*). The purity of the samples was measured by the A_{280}/A_{800} absorbance ratio and typically was between 1.4 and 1.8.

Absorption Spectra. Ground-state absorption spectra were measured with a Shimadzu UV-160 spectrophotometer. For measurements at room temperature, RCs were suspended in 10 mM Tris pH 8.0, 0.1% lauryldimethylamine oxide (LDAO), and 1 mM EDTA. For measurements at 78 K, glycerol was added to give a glycerol/buffer ratio of 2:1 (v:v), and the sample was placed in an acrylic cuvette with a coldfinger immersed in liquid nitrogen; the sample thickness was 1.5 mm. The temperature was measured by a thermocouple inserted directly in the glycerol glass. Because RCs of the double mutant R(L135)E/C(L247)D degraded rapidly after purification, their spectrum was obtained immediately after elution from the Ni column.

Hole-Burning Measurements. Hole-burned spectra were measured at 5 K in a Bruker 120HR FTIR spectrometer with resolution of 1.0 cm^{-1}. A Coherent 899 Ti-sapphire laser with a line width of about 2 GHz (0.067 cm^{-1}) was used for excitation. The RC samples were in a 2:1 (v/v) mixture of glycerol with a buffer solution containing 15 mM Tris pH 8.0, 0.1% LDAO, and 1 mM EDTA and had an absorbance of approximately 1 at 800 nm at 5 K. All spectra were scanned 200 times to achieve a good signal/noise ratio.

All hole spectra presented result from transient conversion of P to its lowest triplet state upon charge recombination of the $P^+H_L^-$ radical ion pair. The transient hole spectrum is the difference between absorption spectra measured with the laser on and off. The persistent hole spectrum (post-burn spectrum minus pre-burn spectrum, both with laser off) was negligible for both the WT and the mutant RCs. Holes were burned in the mutant RC spectra at 17 wavelengths between 908.0 and 877.2 nm (11013 and 11400 cm^{-1}), using three burn intensities (approximately 10, 20, and 40 mW cm^{-2}) at each wavelength. Because WT RCs have been studied previously (*43*), holes were burned in their spectra with only one intensity at each of eight wavelengths; the results were similar to those described by Lyle et al. (*43*). In some of the hole spectra, a narrow (∼1 cm^{-1}) spike due to scattered laser light interfered with the zero-phonon hole. Since the widths of the zero-phonon holes were ∼10 cm^{-1}, the spike could be removed from the hole spectra without significantly affecting the measurements of the hole widths.

The hole spectrum in the low-temperature limit is defined by $A_t(\Omega) - A_{t=0}(\Omega)$, where

$$A_t(\Omega) = \int d\omega G(\omega - \omega_m) L(\Omega - \omega) \times \exp\{-\sigma P \phi L(\omega_B - \omega) t\} \quad (1)$$

is the absorption at frequency Ω following burning at ω_B with photon flux P for time t (*44*). ($A_{t=0}(\Omega)$ is the pre-burn absorption spectrum.) $G(\omega - \omega_m)$ is the Gaussian distribution of zero-phonon line frequencies (the site-distribution function, SDF) centered at ω_m with width (fwhm) Γ_{inh}; and σ and ϕ are the integrated absorption cross-section and the hole-burning quantum yield. $L(\Omega - \omega)$ is the single-site absorp-

tion spectrum

$$L(\Omega - \omega) = e^{-S_t} \sum_{k=1}^{2} \sum_{R=0}^{\infty} \left(\frac{S_k^R}{R!}\right) l_{R,k}(\Omega - \omega - R\bar{\omega}_k) \quad (2)$$

and $L(\omega_B - \omega)$ is the same with ω_B replacing Ω. Here, k labels the phonons that are Franck−Condon active in absorption. On the basis of previous results (*43*), we anticipated that only two low-frequency vibrational modes with center frequencies $\bar{\omega}_1$ ($k = 1$) and $\bar{\omega}_2$ ($k = 2$) and Huang−Rhys factors S_1 and S_2 would be needed to simulate the hole-burned spectra for the P870 band of the mutants (see Results). For the WT RC, $\bar{\omega}_1 \approx 30$ cm^{-1} (*43*). The $\bar{\omega}_2$ mode, with $\bar{\omega}_2 \approx 120$ cm^{-1} in WT RCs, has been referred to as the special-pair marker mode (*43*). S_t is the total Huang−Rhys factor for low-frequency modes ($S_1 + S_2$). The $l_{R,k}$ are line shape functions for transitions involving R phonons of mode k, where $R = 0, 1, 2, ...$ The zero-phonon line shape (l_0) is a Lorentzian with homogeneous width Γ_{hom}. The $l_{1,1}$ profile is described, as previously (*43*), by a Gaussian with width Γ_{G1} on the low-energy side and a Lorentzian with width Γ_{L1} on the high-energy side, so that the fwhm of the one-phonon profile is $(\Gamma_{G1} + \Gamma_{L1})/2$. The $l_{1,2}$ profile is described by a Gaussian with width Γ_{G2}. Eqs 1 and 2 account for overtone transitions and combination bands of the $\bar{\omega}_1$ and $\bar{\omega}_2$ modes. Intramolecular Bchl vibrations were not included in the simulations since they have small Franck−Condon factors (≤ 0.05) and are expected to contribute only to the high-energy tails of the P870 band (*45*).

For each mutant RC studied, the value of $\sigma P \phi t$ required to fit the hole-burned spectrum obtained with the lowest burn intensity (photon flux P_l) was determined. To fit spectra obtained with a higher photon flux (P_h), $\sigma P_l \phi t$ was simply multiplied by P_h/P_l. This led to a satisfactory account of the dependence of the hole spectra on burn intensity, which is possible only if the values of the parameters that define the SDF and the linear electron−phonon coupling are accurate.

Electron-Transfer Kinetics. The femtosecond spectrometer used to measure the electron-transfer kinetics has been described (*46*). Briefly, the output from a cavity-dumped Ti:sapphire laser with a repetition rate of 9.1 kHz was split into two beams with an intensity ratio of 9:1. The more intense pump beam was sent through a pair of dispersion-compensating prisms and was spatially filtered to tune the spectrum to peak at 850 nm with a fwhm of 60 nm (2 nJ per pulse). The weaker probe pulse was focused into a microstructure fiber to generate a white light continuum that was used to measure stimulated emission from the RC. The delay between the pump and the probe pulses was controlled by a variable path length in the pump beam, the polarization between the pump and the probe was set at the magic angle, and both pulses were focused into the sample by an off-axis parabolic mirror. The transmitted probe light continued through a monochromator with a 5 nm band-pass at 930 nm and was detected with a photodiode and a lock-in amplifier, which was synchronized with a chopper that modulated the pump and the probe beams at different frequencies. The second harmonic signal obtained by crossing the pump beam with itself in a 0.1 mm KH_2PO_4 crystal was fit well by a sech$^2(t)$ function with a fwhm of 20 fs. The width of the pump−probe cross-correlation, estimated from the rise time of the pump−probe signal, was approximately 100 fs.

RCs were suspended in 15 mM Tris Hcl, pH 8.0, 0.1% LDAO, and 1 mM EDTA to give an absorbance of 0.2−0.4 at the peak of the P870 band in a 1 mm cuvette. To avoid reexcitation, the sample was held in a spinning cell constructed from a pair of acrylic and BK7 glass disks clamped together with an acrylic ring. One face of the acrylic disk was machined to give an anular sample region with a depth of 1 mm and inner radius of 30 mm. A groove in the acrylic held an O-ring that was sandwiched between the two disks and defined the 40 mm outer radius of the sample region. The sample was injected through a small, tapped hole in the acrylic disk while air escaped from a second hole; both holes then were sealed by O-rings and screws. An aluminum shaft attached to the acrylic disk was coupled by a belt to a motor that rotated the sample at 2 Hz. This allowed the metastable charge-separated state ($P^+Q_A^-$) ample time to recombine to the ground state before re-excitation.

Electrostatics Calculations. Electrostatics calculations were used to estimate the differences in solvation free energy between neutral state (PB_L) and $P^+B_L^-$ and between P and CT states $P_L^+P_M^-$ and $P_L^-P_M^+$. The charge on P^+ in $P^+B_L^-$ was distributed equally between P_L and P_M. The partial charges for the pigments were obtained with QCFF/PI (*47*) and were the same as used in previous calculations of the spectroscopic properties of P^+ (*22*, *23*, *48*).

The change in solvation free energy (potential of mean force) for the reaction $RC^0 \rightarrow RC^{\pm}$, where RC^0 denotes the resting, neutral state of the RC and $RC^{\pm}$ is a given charged or ion-pair state, was calculated as

$$\Delta V_{RC^0 \rightarrow RC^{\pm}} = \sum_i (Q_i^{\pm} - Q_i^0) \sum_j \frac{q_j}{f_{ij} r_{ij}} \quad (3)$$

where Q_i^C is the partial charge on atom i of P_L, P_M, or B_L in state C, q_j is the partial charge on atom j of the protein or crystallographic water molecules, r_{ij} is the distance between atoms i and j, and f_{ij} is a distance-dependent screening function. (Interactions of the electron carriers themselves are omitted on the assumption that they are not affected significantly by the mutations.) Previous studies of the RC (*22*, *23*) and other proteins (*49*) have shown that the dielectric screening of charge−charge interactions between atoms i and j can be represented well by the empirical function

$$f_{ij} = 1 + 60(1 - e^{-\eta r_{ij}}) \quad (4)$$

where η is in the range of 0.1−0.18. We used $\eta = 0.1$. Computer models of the WT and mutant proteins were constructed as described (*21*, *22*), starting with the crystal structure determined by Ermler et al. (*50*). The entire protein was included in these calculations. A Monte Carlo procedure (*22*) was used to average the results over 10 configurations of the polar hydrogens in RC^0. The predicted effect of a mutation on the solvation free energy ($\Delta\Delta V_{RC^0 \rightarrow RC^{\pm}}$) is the difference between the mean values of $\Delta V_{RC^0 \rightarrow RC^{\pm}}$ calculated for the mutant and the WT structures.

Absorption Spectrum Calculations. Absorption spectra for WT and mutant RCs were calculated with an exciton treatment (*24*, *25*) that included the four most pertinent molecular orbitals (HOMO-1, HOMO, LUMO, and LUMO+1) of each of the individual pigments (P_L, P_M, B_L, B_M,

H_L, and H_M) in the crystal structure (*50*). QCFF/PI (*47*) was used to obtain the atomic expansion coefficients for the orbitals. The off-diagonal interaction matrix elements that mix the 32 monomer transitions with each other and with the eight CT transitions of P were calculated using the transition-gradient method (*24*, *25*, *51*) with a cutoff distance of 20 Å, and the full interaction matrix was diagonalized to obtain the transition energies for the complex. This procedure has been used previously to calculate the absorption spectra of WT RCs from several species of bacteria (*24*, *25*). For the geometry found in the *R. sphaeroides* crystal structure (*50*), the exciton−interaction matrix element that couples the Q_y transitions of P_L and P_M was found to be 298 cm^{-1}. Because the residues that were mutated are not in direct contact with the pigments, we assumed that their largest effect would be to change the electrostatic energies of the CT states. This assumption seems reasonable because the change in permanent dipole moment associated with forming the $P_L^+P_M^-$ or $P_L^-P_M^+$ CT state is approximately 18 D, whereas the corresponding change associated with the Q_y transition of monomeric Bchl *a* is less than 2.5 D (*26*−*32*). After adjusting the CT energies to reproduce the energy of the P870 band of WT RCs, we calculated the effects of the mutations on the CT energies using eqs 3 and 4 and used the perturbed CT energies to calculate the absorption spectra of the mutant RCs.

RESULTS

Mutations. The sites of the mutations have been described in a previous study of the midpoint potential (E_m) of P/P^+ (*22*). Arginines L135 and M164 occupy homologous positions on opposite sides of P, with their C_ζ atoms approximately 13 Å from the Mg of the nearer Bchl and 20 Å from the more distant Bchl. They are largely sequestered from the solvent. The hydroxyl group of Tyr L164 may form a hydrogen bond or ion pair with Arg L135. The carboxyl oxygens of Asp L155 are exposed to the solvent and are approximately 14 Å from the Mg atoms of both P_L and P_M. The sulfur of Cys L247 is 6.5 Å from the Mg of P_L and is completely buried from the solvent. Although there is no direct evidence that ionizable residues at these positions are, in fact, ionized, the effects of the mutations on the E_m of P/P^+ suggest strongly that this is the case (*22*).

Absorption Spectra. Figures 1−3 show the electronic absorption spectra of the WT and mutant RCs at 78 K. The absorption maxima of the P870 band at 78 and 295 K are given in Table 1. The largest change in the spectrum occurs in the R(L135)L mutant, where the absorption maximum measured at 78 K shifts to the blue by 284 cm^{-1}. This is one of the largest spectral shifts on record for any mutation that leaves the pigment composition of the RC unaltered. Substitution of Lys, Glu, or Gln for Arg L135 shifts the P870 band in the same direction by 167, 115, and 77 cm^{-1}, respectively. The band also broadens in all these mutants (Figure 1). By contrast, mutations of M164 have little effect on the spectrum (Figure 2). The D(L155)N and Y(L164)F mutations also have little or no effect. The C(L247)K mutation shifts the P870 band to the blue by 245 cm^{-1}, while C(L247)D shifts it in the same direction by 26 cm^{-1}. The R(L135)E/C(L247)K double mutation shifts the band by 219 cm^{-1}, which is considerably less than the sum of the effects of the individual mutations (360 cm^{-1}). On the other hand, the shift caused by the R(L135)E/C(L247)D double mutation (199 cm^{-1}) is larger than the sum of the effects of the individual mutations (141 cm^{-1}). This lack of additivity contrasts with the effects of the same mutations on the E_m (*22*).

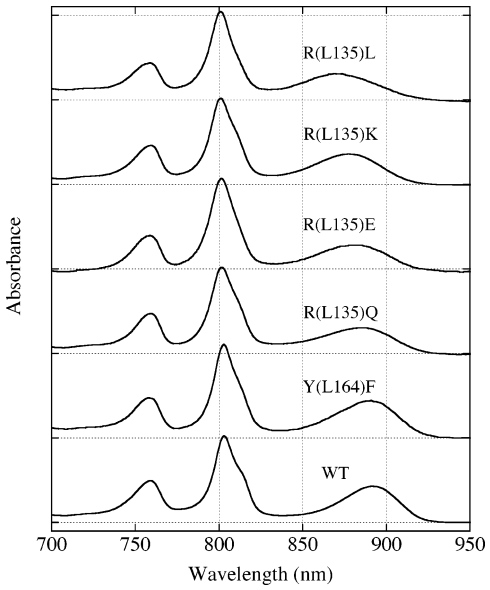

FIGURE 1: Absorption spectra of RCs from WT *R. sphaeroides* and strains with amino acid substitutions for Arg L135 or Tyr L164, measured at 78 K as described in the text.

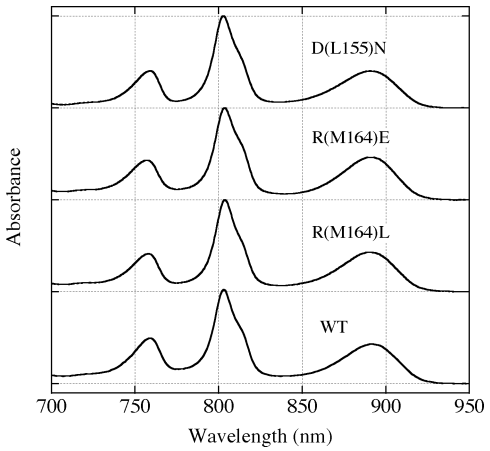

FIGURE 2: Absorption spectra of RCs from WT *R. sphaeroides* and strains with amino acid substitutions for Arg M164 or Asp L155, measured at 78 K as described in the text.

In addition to shifting and broadening the P870 band, some of the mutations cause small blue shifts in the 800 nm band. The peak shifts from 803 nm in WT RCs to 801 nm in the Arg L135 and Cys L247 mutants (Figures 1 and 3) but not in the Arg M164 or Asp L155 mutants (Figure 2). A shoulder on the red side of the 800 nm band is seen in WT and most of the mutant RCs but is less pronounced in R(L135)L and R(L135)E (Figure 1). This shoulder has been assigned to the upper exciton band of the Q_y transitions of P, with contributions from one of the accessory Bchls (*25*, *52*−*54*).

We looked for effects of pH on the room-temperature spectra of WT, R(L135)K, R(L135)Q, R(L135)L, R(L135)E, and R(M164)E RCs. None of the spectra varied significantly with pH between 7.0 and 10.5.

Table 1: Absorption Maxima[a] and Electron-Transfer Time Constants[b]

strain	λ_{max}^{298K} (nm)	$\Delta\Omega_{max}^{298K}$ (cm^{-1})	λ_{max}^{78K} (nm)	$\Delta\Omega_{max}^{78K}$ (cm^{-1})	λ_{max}^{5K} (nm)	$\Delta\Omega_{max}^{5K}$ (cm^{-1})	τ (ps)
wild-type	865	(0)	891	(0)	897	(0)	3.0 ± 0.2
R(L135)K	848	232	878	166	880	221	3.0 ± 0.1
R(L135)L	845	274	869	284	882	196	2.95 ± 0.05
R(L135)Q	859	81	885	76	883	119	2.8 ± 0.05
R(L135)E	852	176	882	115	880	218	3.2 ± 0.3
D(L155)N	863	27	891	0	–[c]	–	3.2 ± 0.14
Y(L164)F	860	67	891	0	–	–	3.1 ± 0.14
R(M164)L	865	0	890	13	–	–	–
R(M164)E	865	0	890	13	897	5	2.76 ± 0.06
C(L247)K	848	232	872	245	–	–	7.03 ± 0.3
C(L247)D	857	108	889	25	–	–	4.7 ± 0.2
R(L135)E/C(L247)K	844	288	874	218	–	–	–
R(L135)E/C(L247)D	846	260	876	192	–	–	–

[a] λ_{max}^{T} is the wavelength of the absorption maximum at temperature T; $\Delta\Omega_{max}^{T}$ is the change in the wavenumber of the absorption maximum relative to WT RCs. [b] τ is the electron-transfer time constant at 295 K, obtained by fitting the pump−probe signal at 930 nm to $S(t) = S(0)\exp(-t/\tau) + C$, where $S(t)$ is the signal at time t and C is a constant. [c] Not determined.

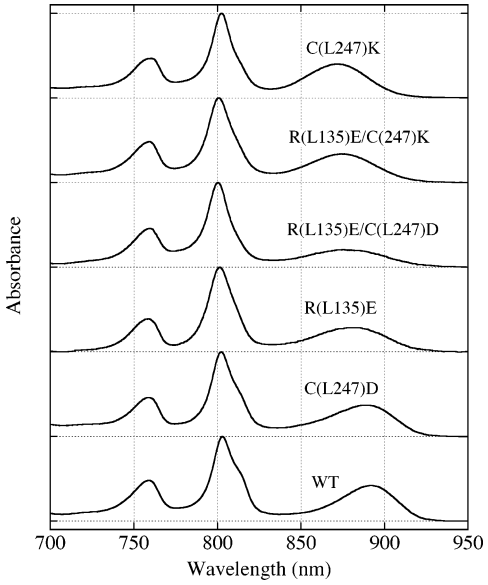

FIGURE 3: Absorption spectra of RCs from WT *R. sphaeroides* and strains with amino acid substitutions for Cys L247 alone or in combination with R(L135)E, measured at 78 K as described in the text.

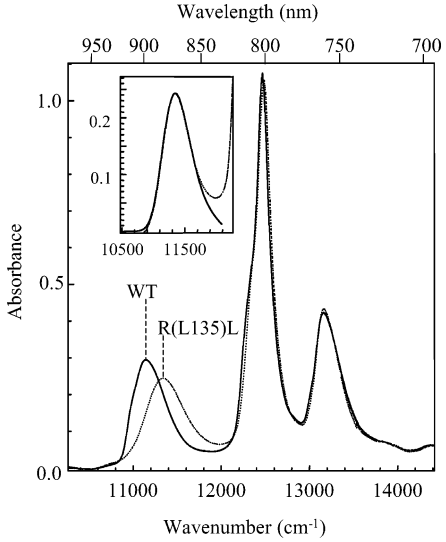

FIGURE 4: Absorption spectra of WT (solid curve) and R(L135)L (dotted) RCs, measured at 5 K as described in the text. The solid curve in the inset is a fit to the R(L135)L spectrum calculated with the parameters given for this mutant in Table 2.

Figure 4 compares the absorption spectra of WT and R(L135)L RCs at 5 K on a wavenumber scale. The spectrum of WT RCs is essentially the same as measured previously at this temperature (*43*). The P870 band of the mutant is broadened and blue-shifted as noted previously for the spectra at 78 K. However, the difference between the peaks of the mutant and WT spectra is smaller at 5 K (about 200 cm^{-1}, as compared to 284 cm^{-1} at 78 K), suggesting that part of the blue shift in the mutant reflects a difference in electron−phonon coupling.

Hole Spectra. To explore the spectroscopic effects of the mutations more closely, we examined the hole-burned spectra obtained by irradiating at various frequencies across the P870 band. Figure 5 shows typical hole spectra for R(L135)L and WT RCs. Similar measurements were made with R(L135)K, R(L135)Q, R(L135)E, and R(M164)E RCs, and the spectra for each strain were fit globally by a process that attempted to reproduce both the shapes and the depths of the holes (see Materials and Methods and ref *44*). Figures 6 and 7 show the measured and simulated hole spectra burned at the lowest and highest burn frequencies for the R(L135)L and R(M164)E RCs. The best-fit parameters for fits to all the spectra are presented in Table 2 along with the corresponding parameters from previous studies of WT RCs (*43*). The same sets of parameter values also were used to simulate the absorption spectra, and as shown in the inset of Figure 4 for R(L135)L RCs, gave good agreement between calculated and experimental spectra across most of the P870 band.

We consider the fits to the hole spectra for the R(M164)E mutant (Figure 7) to be very good. The simulated spectra reproduce the phonon sideband hole structure due to the $\bar{\omega}_1$ and $\bar{\omega}_2$ modes, as well as the combination band ($\bar{\omega}_1 + \bar{\omega}_2$) (Figure 7A). The simulations also correctly predict the absence of a zero-phonon hole (ZPH) when the burn frequency (ω_B) is on the high-energy side of the P870 absorption band (Figure 7B). (The probability of exciting zero-phonon transitions, which lead to the ZPH, decreases with increasing burn frequency, while the probability of exciting phonons increases (*44*).)

The fits to the hole spectra for the R(L135)L mutant (Figure 6A) also are satisfactory except in the high-energy

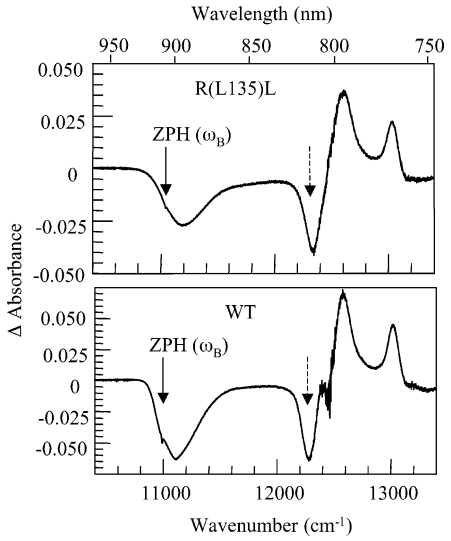

FIGURE 5: Hole spectra of WT (bottom) and R(L135)L (top) RCs, burned by irradiation at frequencies (ω_B) of 10 991 and 11 043 cm^{-1}, respectively (solid arrows). The spectra are the differences between spectra measured at 5 K with and without the burn laser. The negative feature near 11 100 cm^{-1} represents bleaching of the P870 band; the negative feature near 12 300 cm^{-1} (dashed arrow) includes bleaching of a higher-energy exciton band of P and shifts in the absorption bands of B_L and B_M.

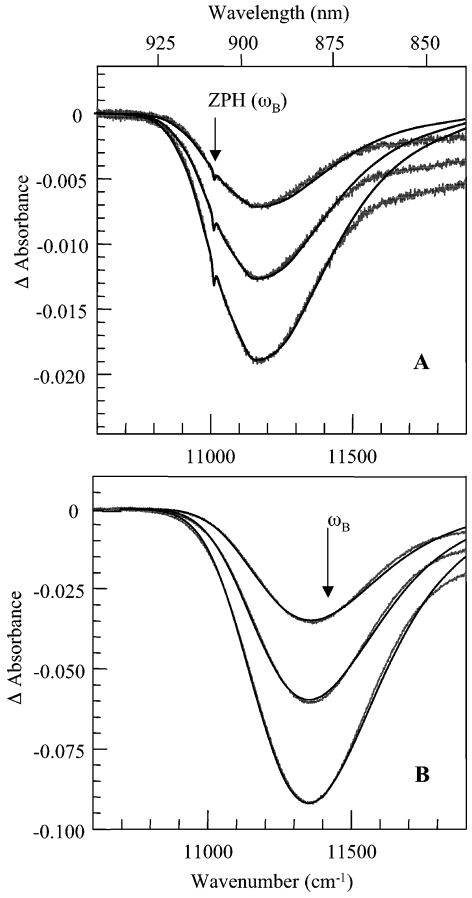

FIGURE 6: Hole spectra of R(L135)L RCs burned at 5 K by irradiation at $\omega_B = 11\,013$ cm^{-1} (A) or 11 400 cm^{-1} (B). The three spectra in each panel were obtained using burn intensities of 10, 20, and 40 mW/cm^2 (top, middle, and bottom, respectively). The spectra calculated with the parameters from Table 2 also are shown (smooth curves).

tail of the band. The discrepancy in this region may be due to neglect of intramolecular Bchl vibrations. Zazubovich et

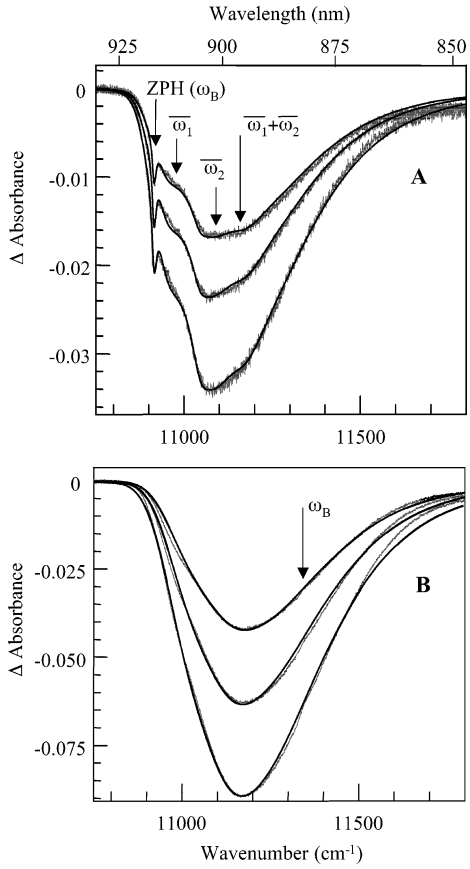

FIGURE 7: Hole spectra of R(M164)E RCs burned at 5 K by irradiation at $\omega_B = 10\,912$ cm^{-1} (A) or 11 337 cm^{-1} (B) with burn intensities of 10, 20, or 40 mW/cm^2 (top, middle, and bottom, respectively). Features representing the $\bar{\omega}_1$, $\bar{\omega}_2$, and combination ($\bar{\omega}_1 + \bar{\omega}_2$) modes are labeled in panel A. The spectra calculated with the parameters from Table 2 also are shown (smooth curves).

al. (*45*) have shown that numerous vibrations with energies between 190 and 1600 cm^{-1} are coupled weakly to the $S_0 \rightarrow Q_y(S_1)$ transition of monomeric Bchl *a*, having Franck−Condon factors ≤0.05. However, the fits in the corresponding region for the R(M164)E mutant (Figure 7A) are quite good, suggesting that the Franck−Condon factors for intramolecular vibrations differ in the two mutants.

The contribution of the ZPH to the hole spectrum was much less pronounced in all the Arg L135 mutants than in WT RCs, as one would expect if electron−phonon coupling is stronger in these mutants. The lower ZPH intensities in the Arg L135 mutants appear to result mainly from larger total Huang−Rhys factors ($S_t = S_1 + S_2$), which are between 3.8 and 4.0 in these mutants as compared to 3.3 in WT RCs (Table 2). The Franck−Condon factor for the ZPH is given by $\exp(-2S_t)$ (*44*), which decreases by a factor of 3 if S_t increases from 3.3 to 3.9. However, the center of the inhomogeneous site-distribution function (ω_m) also increases by 90−160 cm^{-1} in the Arg L135 mutants. The increase in ω_m accounts for about 50% of the total blue shift of the absorption band in R(L135)L, 58% in R(L135)K, 72% in R(L135)E, and 78% in R(L135)Q, with the remainder of the shifts coming from stronger electron−phonon coupling. The fit parameters for R(M164)E RCs, by contrast, are essentially the same as those for WT RCs.

Electron-Transfer Kinetics. The kinetics of electron transfer at 295 K were measured by monitoring the decay of

Table 2: Best-Fit Parameters[a] for Hole Spectra

strain	Γ_{inh} (cm^{-1})	Γ_{hom} (cm^{-1})	ω_m (cm^{-1})	$\bar{\omega}_1$ (cm^{-1})	S_1	Γ_{G1} (cm^{-1})	Γ_{L1} (cm^{-1})	$\bar{\omega}_2$ (cm^{-1})	S_2	Γ_{G2} (cm^{-1})
WT[b]	150	5.8	10 992	30	1.8	30	55	120	1.5	50
R(L135)K	260 ± 20	5 ± 1	$11\,120 \pm 15$	35 ± 5	2.5 ± 0.1	25 ± 5	70 ± 5	135 ± 5	1.5 ± 0.2	40 ± 10
R(L135)L	280 ± 10	5 ± 1	$11\,090 \pm 10$	30 ± 5	2.2 ± 0.1	35 ± 5	65 ± 5	130 ± 5	1.7 ± 0.1	45 ± 5
R(L135)Q	310 ± 10	5 ± 1	$11\,085 \pm 10$	30 ± 5	2.2 ± 0.1	35 ± 5	65 ± 5	130 ± 5	1.7 ± 0.1	45 ± 5
R(L135)E	320 ± 10	5 ± 1	$11\,150 \pm 10$	30 ± 5	2.4 ± 0.1	35 ± 5	65 ± 5	135 ± 5	1.4 ± 0.1	45 ± 5
R(M164)E	130 ± 10	6.5 ± 1	$10\,980 \pm 10$	30 ± 5	2.0 ± 0.1	35 ± 5	55 ± 5	130 ± 5	1.45 ± 0.1	40 ± 5

[a] See Materials and Methods for definitions of the parameters. [b] The values for WT RCs are from Lyle et al. (*43*).

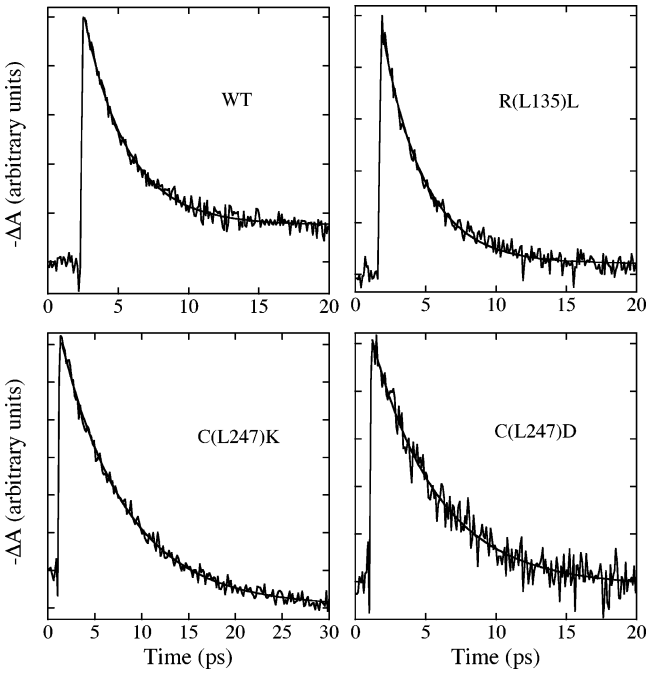

FIGURE 8: Typical transient signals measured at 930 nm for WT and mutant RCs at 295 K (noisy curves) and fits to exponential decay functions (smooth curves).

stimulated emission from P* at 930 nm after excitation at 850 nm. Figure 8 shows typical measurements of the kinetics for WT RCs and several of the mutants, and Table 1 gives the time constants (τ) obtained by fitting the data to a single-exponential function. The WT kinetics were fit well with a time constant of 3.0 ± 0.2 ps. None of the mutations at L135, L155, L164, and M164 had a significant effect on the kinetics, although τ was marginally shorter in the R(M164)E mutant (2.8 ps). The C(L247)D mutation, which introduces a potentially negatively charged residue near P, increased τ to 4.7 ps, whereas replacing the Cys by Lys raised τ to 7.0 ps. Fitting the data to a two-exponential function did not reveal any other significant differences between WT and mutant RCs.

The time constant for the decay of P* at 5 K can be estimated from the hole-burned spectra with the aid of the expression (*55*)

$$\tau = (2\pi\Gamma_{hom}c)^{-1} \quad (5)$$

where $c = 3 \times 10^{10}$ cm s^{-1}, and as above, Γ_{hom} is the homogeneous width of the zero-phonon line (half the observed width of the ZPH). Γ_{hom} was found to be 5 ± 1 cm^{-1} in all the mutants studied except R(M164)E (Table 2). This is the same as in WT RCs within experimental error and gives an electron-transfer time of approximately 1 ps. The R(M164)E mutant exhibited a slightly broader ZPH, corresponding to $\tau \approx 0.8$ ps. (The uncertainty of ± 1 cm^{-1} in the Γ_{hom} values stems mainly from interference by scattered laser light at the ZPH frequency, which depends on the optical quality of the glass. We did not try to optimize the determination of the ZPH width in the present work because our main objective in the hole-burning experiments was to characterize the linear electron−phonon coupling and the site-distribution function for the P870 band in the mutants.)

Calculated Solvation Free Energies and Predicted Effects on the Absorption Spectrum. The expected effects of the mutations on the solvation free energy of the charge-separation process $PB_L \rightarrow P^+B_L^-$ ($\Delta\Delta V_{PB\rightarrow P^+B^-}$) were calculated by using a distance-dependent screening function as described in the Materials and Methods. Column 3 of Table 3 gives the results. For comparison, column 2 gives the measured effects of the mutations on the E_m of P/P^+, which are reproduced well by similar calculations (*22*). The effects on $P^+B_L^-$ should be smaller than the effects on the E_m because electrostatic interactions of the variable amino acid with B_L^- partly balance the interactions with P^+. The guanidino group of Arg L135, for example, is nearly equidistant from P and B_L. Replacing the Arg by Glu lowers the calculated solvation free energy of P^+ by 40 meV (*22*) but increases that of B_L^- by almost the same amount, giving a net change of only −2 meV in $P^+B_L^-$. For Arg M164, which is farther from B_L, the Glu mutation lowers P^+ by 34 meV (*22*) but raises B_L^- by a smaller amount, giving a net change of −13 meV in $P^+B_L^-$. However, the effect of a mutation on the solvation free energy of $P^+B_L^-$ is not simply the sum of the effects on P^+ and B_L^- because the free energies of reorganizing nearby water molecules and polar amino acid side chains are not necessarily additive.

As expected, the predicted effects of most of the mutations on the solvation free energy of charge separation are small, becoming significant only for Y(L164)F, C(L247)K, and C(L247)D, and marginally so for R(M164)E. Because the side chain of Cys L247 is closer to P than to B_L, replacing the Cys by Lys increases the calculated solvation free energy of $P^+B_L^-$, whereas replacing it by Asp has the opposite effect (Table 3, column 3). Examination of the contributions of various factors to the solvation free energies showed that the unexpectedly large effect of the Y(L164)F mutation is an indirect result of reorientation of other polar groups of the protein.

The calculated changes in $\Delta V_{P^*\rightarrow P^+B^-}$ do not include changes in the energy of P*. Estimates of the changes in the solvation free energy of electron transfer from P* in the

Table 3: Calculated Changes in the Solvation Free Energies of $P^+B^-_L$, the CT States of P, and the P870 Band and Measured Shifts in the E_m of P/P^+[a]

strain	ΔE_m (mV)	$\Delta\Delta V_{PB\rightarrow P^+B^-}$ (meV)	$\Delta\Delta V_{P^*\rightarrow P^+B^-}$ (meV)	$\Delta\Delta V_{P\rightarrow P_L^+P_M^-}$ (cm^{-1})	$\Delta\Delta V_{P\rightarrow P_L^-P_M^+}$ (cm^{-1})	$\Delta\Delta V_{P\rightarrow P^*}$ (cm^{-1})
wild-type	(0)	(0)	(0)	(0)	(0)	(0)
R(L135)K	−3	1	−28	27	−8	0
R(L135)L	−20	−2	−36	−88	129	−13
R(L135)Q	−24	0	−10	−98	121	−13
R(L135)E	−37	−2	−24	−192	212	−38
D(L155)N	12	−7	−10	30	−24	0
Y(L164)F	2	−21	−29	23	14	0
R(M164)L	−16	−5	−5	65	−43	0
R(M164)E	−32	−13	−13	165	−118	25
C(L247)K	51	22	−7	272	−268	25
C(L247)D	−40	−21	−34	−332	324	−63

[a] ΔE_m is the measured change in the E_m of P/P^+ in the indicated mutant relative to wild-type RCs; $\Delta\Delta V_{PB\rightarrow P^+B^-}$ and $\Delta\Delta V_{P^*\rightarrow P^+B^-}$ are the calculated changes in the solvation free energies of electron transfer to B_L from, respectively, P and P*; $\Delta\Delta V_{P\rightarrow P_L^+P_M^-}$ and $\Delta\Delta V_{P\rightarrow P_L^-P_M^+}$ are the calculated changes in the solvation free energies of exciting P to its first two CT states ($P_L^+P_M^-$ and $P_L^-P_M^+$); and $\Delta\Delta V_{P\rightarrow P^*}$ is the calculated change in the solvation free energy of raising P to its lowest excited singlet state (P*). All the calculated free energies are the means for 10 structures with polar hydrogens minimized in the neutral state and are expressed as the changes in the mutants relative to WT RCs. The standard errors of the mean are approximately ±24 cm^{-1}. $\Delta\Delta V_{P^*\rightarrow P^+B^-}$ was obtained from $\Delta\Delta V_{PB\rightarrow P^+B^-}$ by subtracting the change in the excitation energy (P → P*), as estimated from the measured shift in the maximum of the P870 band at 295 K. The ΔE_m values are from Johnson et al. (*22*); each of these is an average of three to five measurements and has a standard error of the mean of approximately ±5 mV.

mutants relative to WT RCs ($\Delta\Delta V_{P^*\rightarrow P^+B^-}$) can be obtained from $\Delta\Delta V_{PB\rightarrow P^+B^-}$ by subtracting the measured shifts in the maximum of the P870 absorption band at 295 K (Table 1) and are given in column 4 of Table 3. The increased energy of P* outweighs the increases in $\Delta V_{P^*\rightarrow P^+B^-}$ so that $\Delta\Delta V_{P^*\rightarrow P^+B^-}$ is negative (i.e., electron transfer is more favorable) in all the mutants, ranging from −5 meV in R(M164)L to −36 meV in R(L135)L. This procedure neglects the fact that part of the blue shift of the P870 band in some of the mutants results from increased electron−phonon coupling rather than a shift of the zero-phonon site-distribution function (see above), and it overlooks possible differences in the relaxations of P* prior to electron transfer. The small magnitudes of the calculated energy changes are, nevertheless, consistent with the finding that most of the mutations have little effect on the electron-transfer kinetics.

We used the same treatment to calculate the effects of the mutations on the solvation free energies of the CT states of P ($P_L^+P_M^-$ and $P_L^-P_M^+$). Because mixing of CT transitions with exciton transitions of the Bchls plays an important role in determining the energy of the P870 band, shifts in the CT energies should affect the spectrum. Previous studies of RC mutants have shown that $P_L^+P_M^-$ probably lies below $P_L^-P_M^+$ in energy and mixes more strongly with the Q_y transitions of the Bchls (*30*−*32*). Because Arg L135 is closer to P_L than P_M, while Arg M164 is closer to P_M, the R(L135)E mutation would be expected to lower the energy of $P_L^+P_M^-$, and the R(M164)E mutation should have the opposite effect. As shown in columns 5 and 6 of Table 3, the calculated changes in the solvation free energies of the CT states are in accord with this picture.

To calculate how changes in the CT energies would affect the absorption spectrum, we used an interaction Hamiltonian that included both intramolecular and CT transitions (*24*, *25*). This treatment reproduced the energy of the P870 band for WT RCs at 78 K when the $P_L^+P_M^-$ CT state was placed 13 100 cm^{-1} above the ground state, and $P_L^-P_M^+$ was put 1600 cm^{-1} above $P_L^+P_M^-$. The calculated changes of the CT solvation free energies in the mutants then led to the predicted spectral shifts ($\Delta\Delta V_{P\rightarrow P^*}$) given in column 7 of Table 3. The electrostatic effects of the mutations are predicted to shift the absorption band by only 1−2 nm in most of the mutants. The largest predicted shift is for the C(L247)D mutant and amounts to 5 nm. There was no consistent correlation between the calculated and the observed shifts, and we were not able to improve the agreement by inverting the assumed energies of $P_L^+P_M^-$ and $P_L^-P_M^+$ in WT RCs.

DISCUSSION

Absorption and Hole-Burned Spectra. Some of the mutations described here cause substantial changes in the absorption spectrum of P. Such changes could arise by perturbations of the energies of intramolecular transitions of the individual Bchls, the energies of CT states of P, the electronic coupling of the pigments, or the coupling to vibrations of the protein. Electrostatic perturbations can occur either through direct electrostatic interactions of P with the modified residue or indirectly by reorientation of other polar groups as mentioned previously in connection with the Y(L164)F mutation.

One measure of the electrostatic effects of the mutations was obtained in previous studies of the E_m of P/P^+ (*22*). The E_m decreases systematically as Arg L135 or M164 is replaced by Lys, Leu, Gln, or Glu or if Cys L247 is replaced by Asp; it increases if Cys L247 is replaced by Lys or if Asp L155 is replaced by Gln (see Table 3). The effects of the R(L135)E and C(L247)K mutations on the E_m are close to additive. From the small magnitude of the shifts, Johnson et al. (*22*) concluded that electrostatic interactions of the ionizable amino acid with P and P^+ are strongly screened. Although the mechanism of the screening has not been fully established, it seems likely that electrolytes and water around the modified residues keep the total charge of the system more or less constant. The insensitivity of the absorption spectrum to pH in both WT RCs and the mutants is in accord with this view. Similar observations have been made on water-soluble proteins (*49*) but are perhaps more surprising in an integral membrane protein such as the RC.

In the present study, we found that the shifts in the P870 absorption band were not correlated with the calculated solvation free energies of the CT states of P. For example,

the spectra of the M164 mutant RCs are essentially indistinguishable from those of WT RCs, while the spectra of the L135 mutants are significantly blue-shifted (Table 1); the calculations predict small red shifts for three of the L135 mutants and a blue shift with a comparable magnitude for one of the M164 mutants (Table 3). In addition, the effects of different L135 mutations do not follow the progression Lys < Leu ≈ Gln < Glu that is seen in the E_m (*22*). Leucine causes a larger blue shift than either Lys, Gln, or Glu. These patterns suggest that electrostatic interactions are not the dominant cause of the changes in the spectrum. The changes in the CT solvation energies evidently are too small to allow us to predict the spectral shifts accurately without additional information.

Eastman et al. (*39*) have described small shifts of the P870 band with ionic strength in *R. capsulatus* RCs. A mutant with replacements of six residues near P, B_L, and H_L (*sym*2-1) had a greatly enhanced sensitivity to ionic strength as well as to detergents and temperature. Following earlier suggestions by several groups (*38*, *56*−*58*), Eastman et al. suggested that the spectroscopic changes reflect displacements of an equilibrium between conformers that absorb at different wavelengths, possibly because of a difference in the relative orientations of P_L and P_M (*38*).

The matrix elements that mix intramolecular and CT transitions depend on intermolecular resonance integrals connecting the two Bchls of P (*24*, *25*) and thus could be sensitive to small changes in the geometry of the dimer. In principle, the blue shifts of the P870 band in some of the mutants could result from a weakening of these interactions. This seems unlikely to be the case, however, because both the R(L135)L and R(L135)E mutations decrease the E_m of P/P^+ (*22*), whereas weakening the electronic interactions of the Bchls should increase the E_m. These mutations also have less effect on the absorption spectrum of P^+ than one might expect if the electronic coupling were changed substantially (*23*). Because vibrations that modulate the orbital overlap of the Bchls or the energies of the CT states should be strongly coupled to the absorption, weakening of the electronic interactions also would be expected to reduce the Hwang−Rhys factor (S_t), which is not observed (Table 2).

The hole-burning measurements indicate that the peak of the SDF (ω_m) is about 100 cm^{-1} higher in the R(L135)L mutant than in WT RCs (Table 2). An increase in electron−phonon coupling shifts the Franck−Condon maximum by approximately the same amount, bringing the total shift at 5 K to about 200 cm^{-1} (Figure 4). In addition, the inhomogeneous width of the SDF (Γ_{inh}) almost doubles in the mutant, increasing from 150 to 280 cm^{-1}, and the fwhm of the line shape function for one-phonon transitions of the low-frequency mode [$(\Gamma_{G,1} + \Gamma_{L,1})/2$] increases from 42.5 to 50 cm^{-1} (Table 2). Why these changes are larger in the R(L135) mutants than in R(M164)E and are particularly large in R(L135)L is unclear.

Our analysis of the hole spectra at 5 K does not attempt to account for the shift of the P870 band to the blue at higher temperatures (see Table 1). This temperature dependence has been discussed previously for wild-type RCs and several mutants (*39*, *59*, *60*) and may reflect a temperature-dependent equilibrium between conformers that absorb at different frequencies (*38*, *39*, *56*−*58*). In general, the shift of the absorption peak (Ω_{max}) as the temperature is increased from T_1 to T_2 at constant pressure can be written

$$\Omega(T_2) - \Omega(T_1) = \int_{T_1}^{T_2}\left(\frac{\partial\Omega_{max}}{\partial T}\right)_V dT - 3\left(\frac{\partial\Omega_{max}}{\partial P}\right)_T \int_{T_1}^{T_2} \frac{\alpha}{\kappa} dT \quad (6)$$

where α and κ are, respectively, the linear expansivity and compressibility of the protein, and $(\partial\Omega/\partial P)_T$ is the shift of the absorption frequency with pressure (*59*). The pressure shift is negative in WT RCs and can be related to the CT character of the excited state (*59*). The first term on the right-hand side of eq 6 generally is negative, whereas the second term is positive and makes the dominant contribution. From the absorption maxima given in Table 1, the shift of the spectrum between 78 and 295 K is essentially the same in the R(L135)L, R(L135)Q, R(M164)E, R(M164)L, D(L155)N, and C(L247)K mutants as in WT RCs but is about 20% greater in the R(L135)K, R(L135)E, C(L247)D, and Y(L164)F mutants. It thus also does not correlate in any simple way with the likely electrostatic effects of the mutations. Among the strains for which we measured and fit the hole spectra (see Table 2), the strains with enhanced sensitivity to temperature [R(L135)K and R(L135)E] resemble each other in having somewhat higher values of S_1 and ω_m than the other strains [WT, R(L135)Q, R(L135)L, and R(M164)E]. It is unclear, however, whether the increases in these parameters can account for the greater shift with temperature. The larger values of ω_m would suggest a weakening of the CT contributions to the excited state, which in itself should decrease the temperature dependence of the spectrum.

Electron-Transfer Kinetics. One of the main incentives for this study was to understand how electrostatic interactions with ionized amino acid residues affect the energy of $P^+B_L^-$ relative to P* and thus contribute to the driving force for electron transfer ($-\Delta G°$). Allen and Williams (*61*) have explored the relationship between the E_m of P/P^+, $\Delta G°$, and the electron-transfer rate in a series of hydrogen-bonding mutants, and Haffa et al. (*11*) recently have expanded the study to include mutants with additional anionic amino acids near P. Both groups assumed that the mutations had a negligible effect on B_L^- so that the change in $\Delta G°$ could be calculated simply from the changes in the energy of the P870 band and the E_m of P/P^+. They concluded that making $\Delta G°$ less negative slows charge separation, with a change by 60 meV lowering the rate by 30%, whereas making $\Delta G°$ more negative by up to 50 meV has little effect on the rate. Larger negative changes in $\Delta G°$ increased the rate.

The electrostatics calculations presented in Table 3 include the effects of the mutations on both P^+ and B_L^-. When the changes in the energy of P* also are taken into account, the mutations studied here make the calculated solvation free energy change for the reaction $P^* \rightarrow P^+B_L^-$ more favorable ($\Delta\Delta V_{P^*\rightarrow P^+B^-} < 0$) by amounts ranging from 5 meV in R(M164)L to 34 meV in C(L247)D and 36 meV in R(L135)L. The calculations probably overestimate the magnitude of $\Delta\Delta V_{P^*\rightarrow P^+B^-}$ in some of the mutants, where up to half the blue shift of the P870 band apparently results from increased electron−phonon coupling rather than a shift of the SDF. We also have neglected possible effects of the mutations on relaxations of P* prior to electron transfer. However, corrections for these effects probably would not

amount to more than ±20 meV. Although our analysis of the free energies differs from that used by Allen and Williams (*61*) and Haffa et al. (*11*), our results for the R(L135), R(M164), D(L155), and Y(L164) mutants corroborate their conclusion that making the $\Delta G°$ more negative by amounts less than 50 meV has little effect on the kinetics of electron transfer from P* to H_L (Table 1).

The effects of the L247 mutations, although also small, appear to be more complex. One would expect replacing Cys L247 by Lys or Asp to have opposite effects on the solvation free energy of $P^+B_L^-$ relative to the ground state, and the calculated values agree with this expectation. Neglecting changes in the energy of P* for the moment, the C(L247)D mutation lowers the calculated solvation free energy of $P^+B_L^-$ by 21 meV relative to WT RCs, whereas C(L247)K raises it by 22 meV (Table 3, column 3). However, both the L247 mutations slow the electron-transfer reaction, C(L247)D by a factor of 1.6 and C(L247)K by a factor of 2.3 (Table 1). The slower kinetics in the C(L247)K mutant could possibly be attributed to the increased free energy of $P^+B_L^-$, but the similar kinetics in C(L247)D are more difficult to explain. The calculated decrease in the free energy of $P^+B_L^-$ in C(L247)D is the same as that in Y(L164)F, which has no effect on the kinetics. As mentioned earlier, the previously described mutations that lower the free energy of $P^+B_L^-$ (or, more accurately, lower the E_m of P/P^+) either have no significant effect on the initial electron-transfer kinetics or, when the E_m is lowered by more than about 100 mV, accelerate the reaction (*10*, *11*, *61*).

When the estimated shifts in the energy of P* are included, the calculated change in the free energy of electron transfer relative to WT RCs ($\Delta\Delta V_{P^*\rightarrow P^+B^-}$) becomes negative in both of the L247 mutants. The value for C(L247)D (−34 meV) is similar to those for R(L135)L, R(L135)E, and Y(L164)F, and the value for C(L247)K (−7 meV) is similar to those for R(M164)L, D(L155)N, and R(L135)Q (Table 3, column 4). Since none of these other mutations changed the electron-transfer kinetics, the slower kinetics in both C(L247)K and C(L247)D cannot be explained simply by the calculated energies. Because Cys L247 is relatively close to P, small structural changes accompanying the mutations might weaken the electronic coupling of P and B_L or the coupling of the electron-transfer reaction to vibrational modes of the protein, either of which could slow electron transfer independently of small shifts in the free energies of P* and $P^+B_L^-$.

Conclusions. The mutations studied here were designed to change ionizable groups at various positions around P without greatly altering the electronic or physical structure of the Bchl complex. We showed previously that the resulting changes in the E_m of P/P^+ are reproduced well by a distance-dependent screening function that attenuates Coulombic interactions by a factor of approximately 40 when the charged atoms are separated by 10−12 Å (*22*). Mobile counterions probably keep the total charge of the system essentially constant, so that replacing an Arg residue by Glu, for example, reduces to replacing an Arg^+Cl^- ion pair by Na^+Glu^-. The positions of the counterions will be somewhat different, but the net change in the energy of P^+ will be small. The present study indicates that the electrostatic effects on the free energy of $P^+B_L^-$ also are strongly screened because most of the mutations have no significant effect on the rate of electron transfer. The changes in the solvation free energy of the electron-transfer reaction ($\Delta\Delta V_{P^*\rightarrow P^+B^-}$) calculated by using the same distance-dependent screening function and subtracting the estimated changes in the energy of P* are qualitatively consistent with the experimental results. However, the calculated electrostatic energies do not explain the slowing of electron transfer by about a factor of 2 in the C(L247)K and C(L247)D mutants or the blue shift of the P870 band in some of the Arg L135 and Cys L247 mutants. These effects provide a reminder that site-directed mutations can modify protein structures and vibrational modes in ways that we presently are unable to predict. If electrostatic interactions with the modified residue are well-screened, small structural changes may dominate the observed effects.

REFERENCES

1. Deisenhofer, J., and Norris, J. R. (1993) *The Photosynthetic Reaction Center*, Academic Press, San Diego.
2. Parson, W. W., Chu, Z. T., and Warshel, A. (1990) *Biochim. Biophys. Acta 1017*, 251−272.
3. Laporte, L., Kirmaier, C., Schenck, C. C., and Holten, D. (1995) *Chem. Phys. 197*, 225−237.
4. Roberts, J. A., Holten, D., and Kirmaier, C. (2001) *J. Phys. Chem. B 105*, 5575−5584.
5. Zhang, L. Y., and Friesner, R. A. (1998) *Proc. Natl. Acad. Sci. U.S.A. 95*, 13603−13605.
6. Kolbasov, D., and Scherz, A. (2000) *J. Phys. Chem. B 104*, 1802−1809.
7. Ivashin, N., Källenbring, B., Larsson, S., and Hansson, Ö. (1998) *J. Phys. Chem. B 102*, 5017−5022.
8. Williams, J. C., Alden, R. G., Murchison, H. A., Peloquin, J. M., Woodbury, N. W., and Allen, J. P. (1992) *Biochem. 31*, 11029−11037.
9. Woodbury, N. W., and Allen, J. P. (1995) in *Anoxygenic Photosynthetic Bacteria* (Blankenship, R. E., Madigan, M. T., and Bauer, C. E., Eds.) pp 527−557, Kluwer Academic Publishers, Dordrecht, The Netherlands.
10. Williams, J. C., Haffa, A. L. M., McCulley, J. L., Woodbury, N. W., and Allen, J. P. (2001) *Biochemistry 40*, 15403−15407.
11. Haffa, A. L. M., Lin, S., Katilius, E., Williams, J. C., Taguchi, A. K. W., Allen, J. P., and Woodbury, N. W. (2002) *J. Phys. Chem. B 106*, 7376−7384.
12. Nagarajan, V., Parson, W. W., Gaul, D., and Schenck, C. (1990) *Proc. Natl. Acad. Sci. U.S.A. 87*, 7888−7892.
13. Finkele, U., Lauterwasser, C., Zinth, W., Gray, K. A., and Oesterhelt, D. (1990) *Biochemistry 29*, 8517−8521.
14. Nagarajan, V., Parson, W. W., Davis, D., and Schenck, C. C. (1993) *Biochemistry 32*, 12324−12336.
15. Jia, Y., DiMagno, T. J., Chan, C.-K., Wang, Z., Du, M., Hanson, D. K., Schiffer, M., Norris, J. R., Fleming, G. R., and Popov, M. S. (1993) *J. Phys. Chem. 97*, 13180−13191.
16. Shochat, S., Arlt, T., Francke, C., Gast, P., van Noort, P. I., Otte, S. C., Schelvis, H. P. M., Schmidt, S., Vijgenboom, E., Vrieze, J., Zinth, W., and Hoff, A. J. (1994) *Photosynth. Res. 40*, 55−66.
17. Heller, B. A., Holten, D., and Kirmaier, C. (1995) *Science 269*, 940−945.
18. Katilius, E., Katiliene, Z., Lin, S., Taguchi, A. K. W., and Woodbury, N. W. (2002) *J. Phys. Chem. B 106*, 12344−12350.
19. Gunner, M. R., and Honig, B. (1991) *Proc. Natl. Acad. Sci. U.S.A. 88*, 9151−9155.
20. Gunner, M., Nichols, A., and Honig, B. (1996) *J. Phys. Chem. 100*, 4277−4291.
21. Alden, R. G., Parson, W. W., Chu, Z. T., and Warshel, A. (1995) *J. Am. Chem. Soc. 117*, 12284−12298.
22. Johnson, E., and Parson, W. W. (2002) *Biochemistry 41*, 6483−6494.
23. Johnson, E. T., Müh, F., Nabedryk, E., Williams, J. C., Allen, J. P., Lubitz, W., Breton, J., and Parson, W. W. (2002) *J. Phys. Chem. B 106*, 11859−11869.
24. Warshel, A., and Parson, W. W. (1987) *J. Am. Chem. Soc. 109*, 6143−6152.
25. Parson, W. W., and Warshel, A. (1987) *J. Am. Chem. Soc. 109*, 6152−6163.

26. Ratsep, M., Wu, H. M., Hayes, J. M., and Small, G. J. (1998) *Spectrochim. Acta, Part A 54*, 1279−1289.
27. Ratsep, M., Wu, H. M., Hayes, J. M., Blankenship, R. E., Cogdell, R. J., and Small, G. J. (1998) *J. Phys. Chem. B 102*, 4035−4044.
28. Moore, L. J., Zhou, H., and Boxer, S. G. (1999) *Biochemistry 38*, 11949−11960.
29. Middendorf, T. R., Mazzola, L. T., Lao, K. Q., Steffen, M. A., and Boxer, S. G. (1993) *Biochim. Biophys. Acta 1143*, 223−234.
30. Zhou, Z., and Boxer, S. G. (1997) *J. Phys. Chem. B 101*, 5759−5766.
31. Zhou, H., and Boxer, S. G. (1998) *J. Phys. Chem. B 102*, 9139−9147.
32. Zhou, H., and Boxer, S. G. (1998) *J. Phys. Chem. B 102*, 9148−9160.
33. Murchison, H. A., Alden, R. G., Allen, J. P., Peloquin, J. M., Taguchi, A. K., Woodbury, N. W., and Williams, J. C. (1993) *Biochemistry 32*, 3498−3505.
34. Allen, J. P., Artz, K., Lin, X., Williams, J. C., Ivancich, A., Albouy, D., Mattioli, T. A., Fetsch, A., Kuhn, M., and Lubitz, W. (1996) *Biochemistry 35*, 6612−6619.
35. DiMagno, T. J., Laible, P. D., Reddy, N. R., Small, G. J., Norris, J. R., Schiffer, M., and Hanson, D. K. (1998) *Spectrochim. Acta, Part A 54A*, 1247−1267.
36. Wang, S., Lin, S., Lin, X., Woodbury, N. W., and Allen, J. P. (1994) *Photosynth. Res. 42*, 203−215.
37. Gast, P., Hemelrijk, P. W., Van Gorkom, H. J., and Hoff, A. J. (1996) *Eur. J. Biochem. 239*, 805−809.
38. Müh, F., Rautter, J., and Lubitz, W. (1997) *Biochemistry 36*, 4155−4162.
39. Eastman, J. E., Taguchi, A. K., Lin, S., Jackson, J. A., and Woodbury, N. W. (2000) *Biochem. 39*, 14787−14798.
40. Paddock, M. L., Rongey, S. H., Feher, G., and Okamura, M. Y. (1989) *Proc. Natl. Acad. Sci. U.S.A. 86*, 6602−6606.
41. Feher, G., and Okamura, M. Y. (1978) in *The Photosynthetic Bacteria* (Clayton, R. K., and Sistrom, W. R., Eds.) pp 349−386, Plenum Press, New York.
42. Rautter, J., Lendzian, F., Schulz, C., Fetsch, A., Kuhn, M., Lin, X., Williams, J. C., Allen, J. P., and Lubitz, W. (1995) *Biochemistry 34*, 8130−8143.
43. Lyle, P. A., Kolaczkowski, S. V., and Small, G. J. (1993) *J. Phys. Chem. 97*, 6924−6933.
44. Hayes, J. M., Lyle, P. A., and Small, G. J. (1994) *J. Phys. Chem. 98*, 7337−7341.
45. Zazubovich, V., Tibe, I., and Small, G. J. (2001) *J. Phys. Chem. B 105*, 12410−12417.
46. Nagarajan, V., Johnson, E., Schellenberg, P., Parson, W., and Windeler, R. (2002) *Rev. Sci. Instr. 73*, 4145−4149.
47. Warshel, A. (1973) *Isr. J. Chem. 11*, 709−717.
48. Parson, W. W., Nabedryk, E., and Breton, J. (1992) in *The Photosynthetic Bacterial Reaction Center II. Structure, Spectroscopy and Dynamics* (Breton, J., and Verméglio, A., Eds.) pp 79−88, Plenum Press, New York.
49. Warshel, A., Russell, S. T., and Churg, A. K. (1984) *Proc. Natl. Acad. Sci. U.S.A. 81*, 4785−4789.
50. Ermler, U., Fritzsch, G., Buchanan, S. K., and Michel, H. (1994) *Structure 2*, 925−936.
51. Alden, R. G., Johnson, E., Nagarajan, V., and Parson, W. W. (1997) *J. Phys. Chem. B 101*, 4667−4680.
52. Breton, J. (1985) *Biochim. Biophys. Acta 810*, 235−245.
53. Breton, J. (1988) in *The Photosynthetic Bacteria* (Breton, J., and Verméglio, A., Eds.) pp 59−69, Plenum Press, New York.
54. Reddy, N. R. S., Kolaczkowski, S. V., and Small, G. J. (1993) *Science 260*, 68−71.
55. Small, G. J. (1995) *Chem. Phys. 197*, 239−257.
56. Lous, E. J., and Hoff, A. J. (1986) *Photosynth. Res. 9*, 89−101.
57. Parot, P., Thiery, J., and Verméglio, A. (1987) *Biochim. Biophys. Acta 893*, 294−302.
58. Kirmaier, C., and Holten, D. (1990) *Proc. Natl. Acad. Sci. U.S.A. 87*, 3552−3556.
59. Wu, H.-M., Rätsep, M., Jankowiak, R., Cogdell, R. J., and Small, G. J. (1998) *J. Phys. Chem. B 102*, 4023−4034.
60. Chang, C. H., Hayashi, M., Liang, K. K., Chang, R., and Lin, S. H. (2001) *J. Phys. Chem. B 105*, 1216−1224.
61. Allen, J. P., and Williams, J. C. (1995) *J. Bioenerg. Biomembr. 27*, 275−283.

BI035366D